2013

Defect Distributions and Transport in Nanocomposites: A Theoretical Perspective

Blas Pedro Uberuaga
Los Alamos National Laboratory, blas@lanl.gov

Enrique Martinez
Los Alamos National Laboratory

Zhenxing Bi
Los Alamos National Laboratory

Mujin Zhuo
Los Alamos National Laboratory,

Michael Nastasi
University of Nebraska-Lincoln, mnastasi2@unl.edu

See next page for additional authors

MATERIALS RESEARCH LETTERS

Mater. Res. Lett., 2013
http://dx.doi.org/10.1080/21663831.2013.805442

Taylor & Francis
Taylor & Francis Group

www.tandfonline.com/toc/tmr000/current

Defect Distributions and Transport in Nanocomposites: A Theoretical Perspective

Blas Pedro Uberuaga[a,*], Enrique Martinez[a], Zhenxing Bi[b], Mujin Zhuo[b], Quanxi Jia[b], Michael Nastasi[c], Amit Misra[b] and Alfredo Caro[a]

[a]*Materials Science and Technology Division, Los Alamos National Laboratory, Los Alamos, NM, USA;* [b]*Materials Physics and Applications Division, Los Alamos National Laboratory, Los Alamos, NM, USA;* [c]*Nebraska Center for Energy Sciences Research, University of Nebraska-Lincoln, Lincoln, NE, USA*

(*Received 12 April 2013; final version received 12 May 2013*)

Nanomaterials are attracting great interest for many applications, including radiation tolerance. Most work on radiation effects in nanomaterials has focused on the interfaces. Here, we examine the other aspect of nanocomposites, the dual phase nature. Solving a reaction–diffusion model of irradiated composites, we identify three regimes of steady-state behavior that depend on the defect properties in the two phases. We conclude that defect evolution in one phase depends on the defect properties in the other phase, offering a route to controlling defect evolution in these materials. These results have broad implications for nanomaterials more generally.

Keywords: Nanocomposites, Radiation Effects, Defect Evolution

Nanomaterials are increasingly finding application in a wide range of technologies, from solar energy conversation [1] to fast ion conduction [2] to magnetic materials.[3] For many of these applications, the critical factor that favors nanomaterials over larger grained alternatives is the behavior of defects within the material, either because of enhanced mass transport or increased reactivity of defects. These factors are particularly important for developing radiation-tolerant materials, where enhanced defect recombination and annihilation result in overall improved resistance to radiation-induced damage mechanisms, such as swelling [4] and embrittlement.[5]

Much attention has been devoted to the role that the interfaces in nanocomposites play on the radiation tolerance of nanocomposites.[6,7] It has been long understood that these interfaces can act as sinks for radiation-induced defects and mitigate their accumulation.[8–10] More recent work has connected the propensity for interfaces to interact with defects and gases with the atomic structure of those interfaces, offering new possibilities for engineering the radiation tolerance of materials by designing materials with specific types of interfaces.[11] Given that nanomaterials maximize the density of such interfaces, the field of radiation damage in nanomaterials has seen considerable growth in recent years.[12–16]

One aspect that has been overlooked is the role that the composite phases themselves have on the defect evolution in the material. To date, most attention has been focused on the role of the interfaces [17] and not the component phases. In series of recent papers,[18–20] (Z. Bi, private communication) the radiation damage behavior in a special class of oxide heterointerfaces, interfaces that are nearly perfectly coherent, were examined both experimentally and theoretically. It was found that, under similar radiation conditions, the response of a given material on one side of the interface was very sensitive to the composition of the material on the other side of the interface, as illustrated in Figure 1. In particular, the behavior of $SrTiO_3$ (STO) in these three experiments is very different. In one case ($TiO_2/SrTiO_3$), a thin amorphous layer forms on the STO side. In the case of $BaTiO_3$/STO, no amorphization is observed. Finally, in the case of STO/$LaAlO_3$, the STO side amorphizes to a great extent. In the TiO_2/STO sample, the formation of a defect denuded zone at the interface on the TiO_2 side was also observed. This wide variety in behavior occurs even though atomistic modeling revealed that there were

*Corresponding author. Email: blas@buber.net, blas@lanl.gov

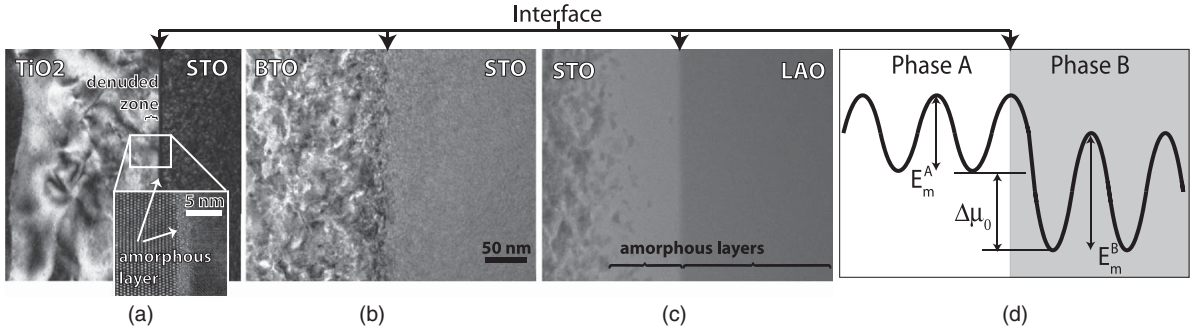

Figure 1. Examples of the irradiation response of different oxide heterointerfaces: (a) $TiO_2/SrTiO_3$, (b) $BaTiO_3/SrTiO_3$, and (c) $SrTiO_3/LaAlO_3$. In each case, the film thickness was between 250 and 300 nm and the irradiation conditions were chosen such that about 3–4 dpa occurred just under the interface. In each case, the energy of the implanted Ne and the total fluence were (top) 250 keV, 1.11×10^{16} ions/cm^2, (middle) 300 keV, 1.55×10^{16} ions/cm^2, and (bottom) 260 keV, 8.23×10^{15} ions/cm^2. The positions of the denuded zone and amorphous layers are labeled. The scale bar for all three images is the same. (d) Schematic of the typical energetic landscape for point defects as determined from atomistic calculations. Details about these experiments and the corresponding atomistic calculations can be found in [18,20] (Z. Bi, private communication).

no thermodynamic trap states for defects at these interfaces. Rather, it was hypothesized that the controlling parameters were the defect properties within each of the bulk phases and that the interface simply acted as a transition point between the two materials. In particular, it was argued that the formation and migration energies of defects within each phase determined the eventual behavior at the interface. The formation energies dictated the direction of flow of defects, while the migration energies dictated the rate of defect flow.

Here, we solve a reaction–diffusion model of point defect evolution in the presence of an interface between two materials in an arbitrary composite. We demonstrate that the behavior of defects at the interface can be quite complex, with multiple steady-state regimes possible. Transient behavior leading to steady-state conditions can be even more complex. We conclude that the defect evolution and distributions within a nanocomposite are very sensitive to the properties of the component phases. This has important consequences for not only radiation tolerance, but also other applications where defect behavior is critical.

The parameters of the model consist of the defect properties within each material: the formation energy (or chemical potential at $T = 0$ K, μ_0) and the migration energy E^{m}, both of which depend on which phase the defect resides in. Two types of defects are considered, nominally an interstitial and a vacancy. The simulation is spatially discretized into cells in which the local defect concentration is tracked. The defect population within a cell j at time t can change with time via an explicit finite difference discretization scheme for the diffusion equation (shown for interstitials I, but an equivalent equation exists for vacancies V):

$$\begin{aligned} c_I^j(t) =& c_I^j(t-\delta t) + S_I - K_{VI} c_I^j(t-\delta t) c_V^j(t-\delta t) \\ &+ c_I^{j+1}(t-\delta t) k_I^{j+1\to j} + c_I^{j-1}(t-\delta t) k_I^{j-1\to j} \\ &- c_I^j(t-\delta t) k_I^{j\to j+1} - c_I^j(t-\delta t) k_I^{j\to j-1}, \quad (1) \end{aligned}$$

where c_I^j is the concentration of interstitials in cell j, S_I is the production rate of interstitials, K_{VI} is the rate coefficient for interstitial–vacancy annihilation, and k are rates for defects to move from one cell to a neighboring cell. $k = \nu_0 \exp(-E^{\mathrm{m}}/k_{\mathrm{B}}T)$, where k_{B} is the Boltzmann constant, T is temperature, ν_0 is a rate prefactor, and E^{m} are the migration energies. In each cell, the migration energy for the given defect is determined by its value in the given phase; for cells just on either side of the interface, the migration energies are modified by the difference in chemical potential μ_0 for the defect. The basic landscape of the model is schematically illustrated in Figure 1(d). Note that this model does not contain any special behavior at the interface beyond a simple transition point between one material with one set of defect properties to another. Distances and times are given in arbitrary units as a choice of length scale sets the time scale via the ratio $\mathrm{d}t/\mathrm{d}x^2$. Thus, changing the relevant length scale simply scales the time scale but the resulting curve is unchanged. For the simulations reported in Figs. 2–4, K_{IV} was 0.001 cm^3/s, S (both species) was 0.001/cm^3/s, υ_0 was 0.04 cm^2/s, and $T = 1,250$ K. For the simulations reported in Fig. 6, K_{IV} was 0.001 cm^3/s, S (both species) was 0.02/cm^3/s, υ_0 was 0.04 cm^2/s, and $T = 300$ K.

We first examine the behavior predicted by the model as a function of the parameters that describe the basic material properties. The values of the parameters for all of the figures are given in Table 1. We identify three regimes of steady-state behavior that describe different evolution of the defects at the interface. These regimes are illustrated in Figure 2. In the first regime, the concentrations of both defects are enhanced on one side of the interface and depleted on the other, relative to the steady-state concentration in the center of the layer. In the second regime, both defects achieve a flat concentration profile in each layer, but in one layer interstitials have a higher concentration than vacancies, and the opposite is true in the other layer. The third regime is in some sense an intermediate case in which there is slight enhancement and

Table 1. Model parameters used to generate the results in the various figures.

	Figure					
Parameter	2(a)	2(b)	2(c)	3(a)	3(b)	4
E_V^{mA}	0.75	0.75	0.75	C	1.0	1.25
E_I^{mA}	1.0	1.0	1.25	C	1.0	1.25
E_V^{mB}	1.0	1.0	1.0	C	1.0	1.0
E_I^{mB}	1.0	1.0	1.0	C	1.0	1.0
$\Delta\mu_{0V}$	0.25	0.25	0.25	0.2	C	0.25
$\Delta\mu_{0I}$	0.25	−0.25	0.25	0.2	$-C$	−0.25

Notes: $\Delta\mu_0$ are defined relative to phase B: $\Delta\mu_0 = \mu_0^{\mathrm{A}} - \mu_0^{\mathrm{B}}$. C indicates that the variable was varied in the plot and that all parameters had the same value. Negative values of chemical potential indicate that the defect prefers to reside in phase A.

depletion of one defect at the interface, while the other defect sees no discontinuous spike at the interface. It is interesting to note that there is no regime in which the interstitial concentration is enhanced at the interface on one side and the vacancy on the other side.

In the first regime, the chemical potential differences of both defects are the same, such that both defects have a thermodynamic tendency to flow from phase A to phase B. Because the annihilation rate is smaller, in these simulations, than the diffusion rate, as defects flow from A to B, there is a depletion of both defects in the interfacial region of phase A and an accumulation in phase B, which persists independent of the rate of flow of defects within the material. That is, even if the defects flow quickly in both materials, the concentration spikes still exist. The differences in the behavior of the two defects in the different regions of the material are dictated by the different kinetic properties of each. Interestingly, even though both defects have the same thermodynamic driving force to move from phase A to phase B, because of the differences in kinetics, the defect populations are inverted in each phase.

In regime 2, the chemical potential is equal but opposite for both defects and the thermodynamic tendency for flow is also opposite. In this case, annihilation is small because there is never any appreciable concentration of one or the other defect in a given phase of the composite.

Finally, regime 3 represents an intermediate case. Here, one of the defects is depleted on one side of the interface and enriched on the other, but the second defect concentration only exhibits depletion and, unlike in the other cases, is continuous across the interface. While the generic behavior is reminiscent of regime 2, rather than being driven by the differences in thermodynamic

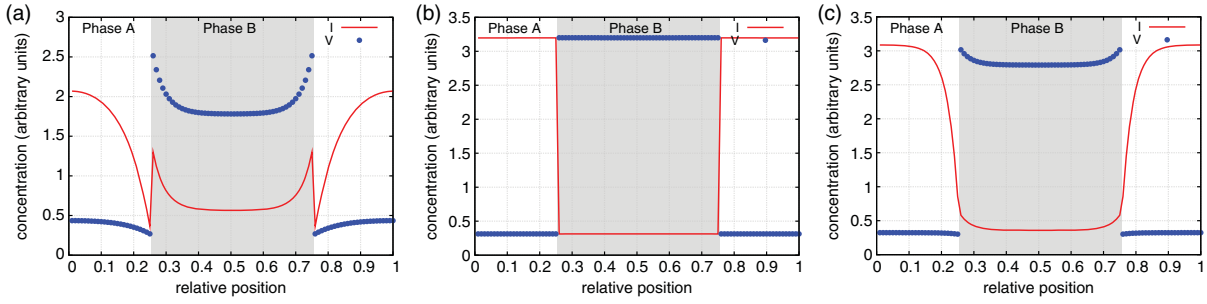

Figure 2. Three regimes of defect behavior at the composite interface discussed in the text: (a) regime 1, (b) regime 2, and (c) regime 3. The shaded region represents one phase, while the white region is the other phase. Interstitial concentrations are indicated by the solid lines, while vacancy concentrations are indicated by the points.

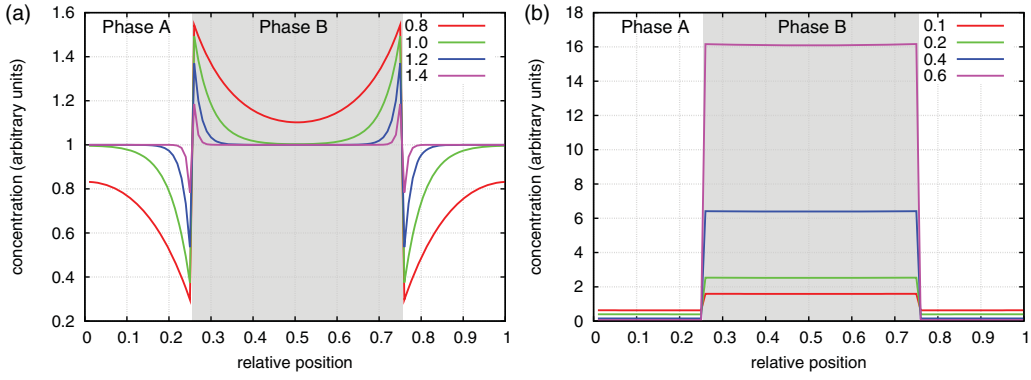

Figure 3. (a) Steady-state concentrations for interstitials as a function of migration barriers, depicted in the legend and having units of eV. The parameters are chosen such that the vacancy concentrations are identical. (b) Steady-state concentrations for interstitials as a function of chemical potential, depicted in the legend and having units of eV.

properties of the defects in the two phases, the concentration profiles are driven by the kinetics: both defects have the same thermodynamic driving force to flow from phase A to phase B, but the concentrations are inverted with respect to one another.

Figure 2(a), in addition to demonstrating non-uniform defect concentrations at the interface, also reveals that the defect concentrations in the center of each layer is very sensitive to the defect kinetics. In this particular case, the chemical potentials of each defect are identical, the only differences are in the migration energies. This suggests that the steady-state concentration of defects in one phase of the composite can be controlled to a high degree by the kinetic properties in the other phase. This is demonstrated more explicitly in Figure 3, which shows the steady-state concentrations of interstitials for a series of cases in which the chemical potential differences for both defects are equal and held constant and all of the migration energies are equal but varied ($E_I^{mA} = E_I^{mB} = E_V^{mA} = E_V^{mB}$). By varying the migration energies by 0.6 eV, the behavior at the interface and the average concentration in each phase changes significantly, with more defects flowing from phase A to phase B as the kinetics are increased.

Similarly, in cases when the thermodynamic driving forces for flow of the two defects is in opposite directions ($\Delta\mu_{0V} = -\Delta\mu_{0I}$), there is a strong dependence of the defect content in one material on the relative defect formation energies in the other material, as would be expected. This is illustrated in Figure 3(b) in which the kinetic properties of all defects are held constant while the differences in chemical potentials are varied. In this case, in which the defect thermodynamics dominate over the kinetics, very large changes in defect content are possible. Again, this points to the fact that the defect population in one phase can be influenced by the properties of the neighboring phase.

All of the above discussion refers to results of the model once it has reached a steady-state condition. In many materials examined in laboratory conditions where temperatures might be moderate, the material does not often reach steady state. This is particularly true of oxide ceramics in which migration energies are often quite high and many defects produced under irradiation have very little mobility. To better understand how the transient behavior might differ from the steady-state behavior, in Figure 4 we examine a case in which the steady-state behavior is characteristic of regime 2, but the transient behavior exhibits much more complex defect behavior. As a function of time, defect concentrations at the interface become significantly enhanced and depleted. In particular, the defect enhancement at the interface is higher than the eventually steady-state concentrations. Thus, in this particular case, even if the material is able to accommodate the steady-state defect concentrations, transient spikes might lead to situations

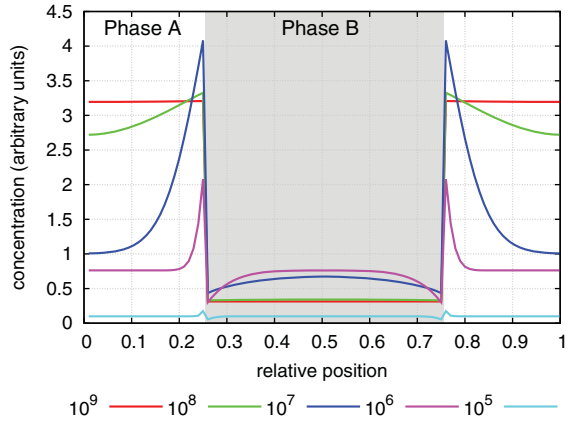

Figure 4. Defect concentrations as a function of time. The values of time, in arbitrary units, are given in the legend and represent an order of magnitude increase in simulation time for each curve.

in which the material fails due to unsustainable levels of defects.

Finally, to better understand how the properties of defects in one phase influence the behavior in the other phase, we consider another set of simulations meant to mimic a composite in which one phase is Cu and the other phase is an arbitrary material. Thus, in the Cu phase, we set $E_V^m = 0.7$ eV and $E_I^m = 0.1$ eV. The properties of the defects in phase A are then systematically varied. The resulting concentrations of interstitials and vacancies at the interface in the Cu phase at steady state are reported in Figure 5. As can be seen from the figure, the defect concentrations in the Cu phase vary significantly with the properties of phase A, with interstitial concentrations varying for a given set of chemical potentials by as much as 250 times and vacancy concentrations by as much as 500 times. Further, as the relative chemical potential of defects are varied, peak concentrations of defects vary by about two orders of magnitude. Thus, there is a very strong coupling between the defect response in the Cu phase with the defect properties in phase A.

These results lead to the conclusion that defect evolution in composites is critically dependent on the composition of the composite. Further, the radiation damage response of the composite cannot be viewed as the isolated response of each component material. It is precisely through their coupling, even independent of the properties of the interfaces that connect them, that their response is determined.

This model is rather basic and neglects a number of features that would be present in real materials. First, we assume that defects of all types can exist in both phases of the composite. This might be reasonable for complex oxide composites such as $TiO_2/SrTiO_3$ in which, for example, Ti interstitials and vacancies can exist in both phases. It would also be reasonable for amorphous/crystalline composites or materials composed of, for example, Fe in both fcc and bcc phases.

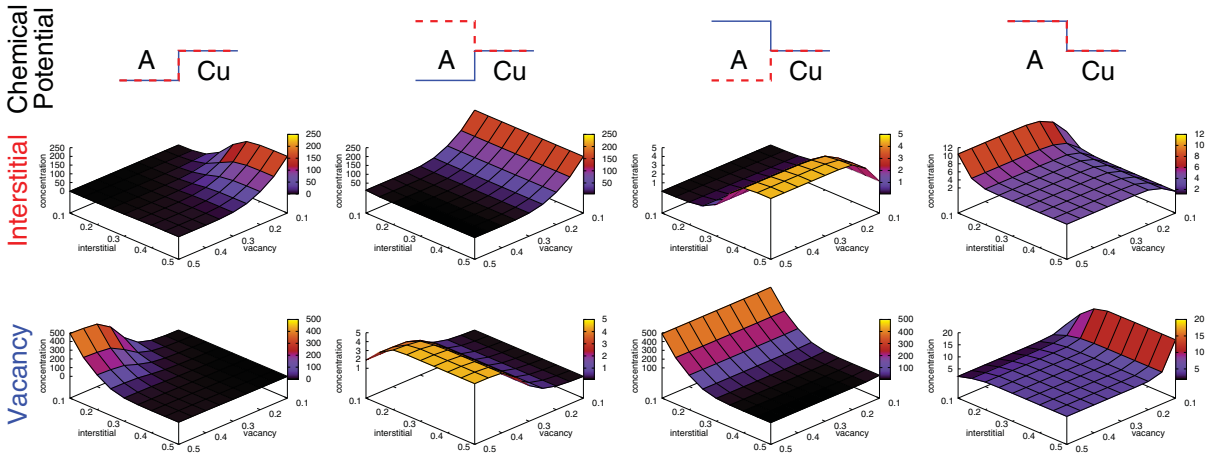

Figure 5. Dependence on the interstitial and vacancy concentrations on the 'Cu' side of the interface as a function of the properties of phase A. The axes in each figure are the migration energies of interstitials and vacancies in phase A, in eV. The schematic differences in chemical potential are listed at the top where the dashed (red) line indicates the relative chemical potential for interstitials and the solid (blue) line is that for vacancies.

However, more generally, a vacancy in one phase can only exist in the other by considering the enthalpy of mixing (consider, for example, a Nb vacancy in a Cu/Nb composite). In such a case, as the vacancy moves from one phase to the other, a backward flux of atoms of the second phase would cross the interface, leading to intermixing. We have also assumed a dilute limit in which the only defect–defect interaction is interstitial–vacancy annihilation. In real systems, defects can agglomerate, leading to extended defect clusters that have their own kinetic and thermodynamic properties. Finally, we have, in the end, only explored a relatively small region of the possible phase space of the model. We have not systematically examined the role of the defect production rate, internal sinks (such as dislocations), or the strength of the interstitial–vacancy annihilation on the predicted results. Further, for reasons of numerical stability, we have only varied E_m and $\Delta\mu_0$ within a relatively small window. The relevant migration energies and chemical potentials in many oxide composites are much larger. Thus, there could be other regimes present in the model. That said, once E_m is large enough, for example, increasing it further will not influence the results as the defects have crossed a threshold of mobility. We therefore expect that the results presented here represent the range of behavior possible in the system.

In spite of these simplifying assumptions, we expect that the basic insight provided by this simple model will have some applicability to composites more generally and provide new avenues for exploring the radiation tolerance of complex materials. The model reproduces the basic features seen in the experiments summarized in Figure 1, suggesting that, even in its simplicity, this model accounts for the basic processes that govern the behavior seen in these materials. In regime 1, there is a depletion of defects on one side of the interface (a 'denuded zone') and an enhancement on the other side, which could lead to amorphization, as found in $TiO_2/SrTiO_3$ (Figure 1(a)). If the chemical potentials are equal $\Delta\mu_0 = 0$, there is no flow of defects from one phase to the other and no special behavior at the interface, as in $BaTiO_3/SrTiO_3$. That said, there are certainly a number of other factors that influence radiation damage in nanomaterials, including the mechanisms for recombination,[21] the energetics of the interfaces themselves,[17] and the role of trap states at the interfaces.[22–24] A comprehensive model of radiation damage evolution in nanomaterials would need to account for all of these factors. The simple model presented here, however, suggests that the relative properties of point defects in the different phases of a nanocomposite are of great importance.

It is useful to compare the behavior predicted by this model with literature results on irradiation studies of composites. Relatively few studies of irradiation effects in composites have analyzed the relative radiation tolerance of the two phases. One particularly interesting example involves ZrO_2. Bulk ZrO_2 is very difficult to amorphize, withstanding doses of 680 dpa,[25] while nanocrystalline ZrO_2 resists amorphization up to doses of at least 80 dpa.[26] In contrast, ZrO_2 nanoparticles embedded in a SiO_2 matrix were observed to amorphize by doses as little as 0.5 dpa.[27] This has been rationalized as a consequence of the high energy of the interfaces in the composite when compared with the nanocrystalline material.[17,27] However, the present model would suggest that there is likely a thermodynamic driving force for defects to flow from one phase to the other, possibly destabilizing the ZrO_2 phase and leading to its quick amorphization. Such a driving force would not exist in the nanocrystalline material. Further, it has been proposed that the behavior of He in oxide dispersion strengthened steels is dictated by a similar energy

landscape, albeit one that also involves a trap state at the interface.[28] Thus, He implantation experiments might provide another avenue for validating the premises of the model presented here.

Certainly, these results have important consequences for the development of nanocomposites for radiation tolerance, as the defect distributions within the material can be controlled to a great degree simply by choosing the appropriate component phases. However, the impact of these results is much broader. Any application of nanocomposites in which defect transport or distributions are critical will be affected by the flow of defects between the component phases, as determined by the diffusivities of the defects, and the relative chemical potentials of the defects. Indeed, a similar model has been proposed for mechanical alloying in Cu–Al composites.[29] In addition, defect content and distributions are clearly important for the performance of fast ion conductors. Thus, there is great promise in engineering nanocomposites for such applications by optimizing the choice of the component phases.

To conclude, using a simple reaction–diffusion model, we have shown that the defect evolution in composites is very complex, depending critically on the composition of the composite. By varying the properties of one phase within the composite, the defect evolution within the other phase can be modified to a very high degree. This is true even in simple composites in which the interface has no special interaction with defects and merely acts as a transition point between two materials. These results suggest that the radiation damage of a composite material can be tailored by choosing the appropriate component materials. In particular, the radiation tolerance of a phase that has relatively poor radiation tolerance in single-phase form might be significantly enhanced by the appropriate selection of a second phase. As an approach to controlling radiation damage in complex materials, changing the component materials may be much more straightforward than engineering specific types of interfaces and, thus, these results have significant potential in leading to new radiation-tolerant composites.

Acknowledgements This work was supported as part of the Center for Materials at Irradiation and Mechanical Extremes, an Energy Frontier Research Center funded by the U.S. Department of Energy (DOE), Office of Science, Office of Basic Energy Sciences under Award Number 2008LANL1026. Los Alamos National Laboratory, an affirmative action equal opportunity employer, is operated by Los Alamos National Security, LLC, for the National Nuclear Security Administration of the U.S. DOE under contract DE-AC52-06NA25396.

References

[1] Kamat PV. Meeting the clean energy demand: nanostructure architectures for solar energy conversion. J Phys Chem C. 2007;111(7):2834–2860.

[2] Tuller HL. Ionic conduction in nanocrystalline materials. Solid State Ion. 2000;131(1–2):143–157.

[3] Herzer G. Modern soft magnets: amorphous and nanocrystalline materials. Acta Mat. 2013;61(3):718–734.

[4] Garner FA. Irradiation performance of cladding and structural steels in liquid metal reactors, Vol. 10A of Materials Science and Technology: A Comprehensive Treatment. Weinheim: VCH Publishers; 1994. Chapter 6, p. 419–543.

[5] Porter DL, Garner FA. Irradiation creep and embrittlement behavior in AlSi 316 stainless-steel at very high neutron fluences. J Nucl Mater. 1988:159;114–121.

[6] Misra A, Demkowicz MJ, Zhang X, Hoagland RG. The radiation damage tolerance of ultra-high strength nanolayered composites. JOM. 2007;59:62–65.

[7] Odette GR, Alinger MJ, Wirth BD. Recent developments in irradiation-resistant steels. Annu Rev Mater Res. 2008:38;471–503.

[8] Siegel RW, Chang SM, Balluffi RW. Vacancy loss at grain-boundaries in quenched polycrystalline gold. Acta Metall. 1980:28(3);249–257.

[9] Thorsen PA, Bilde-Sorensen JB, Singh BN. Bubble formation at grain boundaries in helium implanted copper. Scr Mater. 2004:51(6);557–560.

[10] Barnes RS, Redding GB, Cottrell AH. The observation of vacancy sources in metals. Philos Mag. 1958:3(25);97–99.

[11] Demkowicz MJ, Hoagland RG, Hirth JP. Interface structure and radiation damage resistance in Cu–Nb multilayer nanocomposites. Phys Rev Lett. 2008:100(13); 136102-1–4.

[12] Yamada R, Zinkle SJ, Pells GP. Defect formation in ion-irradiated Al_2O_3 and $MgAl_2O_4$—effects of grain-boundaries and fusion transmutation products. J Nucl Mater. 1992:191;640–644.

[13] Chimi Y, Iwase A, Ishikawa N, Kobiyama M, Inami T, Okuda S. Accumulation and recovery of defects in ion-irradiated nanocrystalline gold. J Nucl Mater. 2001:297(3);355–357.

[14] Swaminathan N, Kamenski PJ, Morgan D, Szlufarska I. Effects of grain size and grain boundaries on defect production in nanocrystalline 3C-SiC. Acta Mater. 2010:58(8);2843–2853.

[15] Shen TD, Feng S, Tang M, Valdez JA, Wang YQ, Sickafus KE. Enhanced radiation tolerance in nanocrystalline $MgGa_2O_4$. Appl Phys Lett. 2007:90(26);263115.

[16] Landau P, Guo Q, Harrat K, Greer JR. The effect of he implantation on the tensile properties and microstructures of Cu/Fe nano-bicrystals. Adv Funct Mater. 2013:23(10);1281–1288.

[17] Shen TD. Radiation tolerance in a nanostructure: is smaller better? Nucl Instrum Methods Phys Res B. 2008:266(6);921–925.

[18] Zhuo MJ, Fu EG, Yan L, Wang YQ, Zhang YY, Dickerson RM, Uberuaga BP, Misra A, Nastasi M, Jia QX. Interface-enhanced defect absorption between epitaxial anatase TiO_2 film and single crystal $SrTiO_3$. Scr. Mater. 2011:65(9);807–810.

[19] Zhuo MJ, Uberuaga BP, Yan L, Fu EG, Dickerson RM, Wang YQ, Misra A, Nastasi M, Jia QX. Radiation damage at the coherent anatase $TiO_2/SrTiO_3$ interface under Ne ion irradiation. J Nucl Mater. 2012:429(1–3);177–184.

[20] Bi Z, Uberuaga BP, Vernon LJ, Fu E, Wang YQ, Li N, Wang H, Misra A, Jia QX. Radiation damage in heteroepitaxial $BaTiO_3$ thin films on $SrTiO_3$ under Ne ion irradiation. J Appl Phys. 2013:113(2);023513.

[21] Swaminathan N, Morgan D, Szlufarska, I. Role of recombination kinetics and grain size in radiation-induced amorphization. Phys Rev B. 2012:86(21);214110.

[22] Demkowicz MJ, Misra A, Caro A. The role of interface structure in controlling high helium concentrations. Curr Opin Solid State Mater Sci. 2012:16(3); 101–108.
[23] Kolluri K, Demkowicz MJ. Formation, migration, and clustering of delocalized vacancies and interstitials at a solid-state semicoherent interface. Phys Rev B. 2012:85(20);205416.
[24] Tschopp MA, Solanki KN, Gao F, Sun X, Khaleel MA, Horstmeyer MF. Probing grain boundary sink strength at the nanoscale: energetics and length scales of vacancy and interstitial absorption by grain boundaries in alpha-Fe. Phys Rev B. 2012:85(6);064108.
[25] Sickafus KE, Matzke H, Hartmann T, Yasuda K, Valdez JA, Chodak P, Nastasi M, Verall RA. Radiation damage effects in zirconia. J Nucl Mater. 1999:274(1–2); 66–77.
[26] Rose M, Gorzawski G, Miehe G, Balogh AG. Phase stability of nanostructured materials under heavy ion irradiation. Nanostruct Mater. 1995:6(5–8);731–734.
[27] Meldrum A, Boatner LA, Ewing RC. Nanocrystalline zirconia can be amorphized by ion irradiation. Phys Rev Lett. 2002;88(20):025503-1–4.
[28] Erhart PJ. A first-principles study of helium storage in oxides and at oxide–iron interfaces. Appl Phys. 2012:111(11);113502.
[29] Khina BB, Solpan I, Lovshenko GF. Modelling accelerated solid-state diffusion under the action of intensive plastic deformation. J Mater Sci. 2004:39(16–17);5135–5318.